Validation of a Novel Parallel-Actuated Shoulder Exoskeleton Robot for the Characterization of Human Shoulder Impedance

Dongjune Chang, Justin Hunt, John Atkins and Hyunglae Lee*, *IEEE Member*

Abstract— **This study validates the effectiveness of a recently developed parallel-actuated shoulder exoskeleton robot for the purpose of characterizing the neuromuscular properties of the human shoulder joint. In particular, shoulder mechanical impedance was quantified, which can be represented by a 2nd order system consisting of spring, damper and inertia. The shoulder exoskeleton robot, which utilizes a new type of 4-bar spherical parallel manipulator (4B-SPM), has inherently low inertia and as a result can provide fast perturbations that are often essential for characterizing neuromuscular properties. The robot was first evaluated by using a physical shoulder mockup with adjustable and known spring and mass properties. The results of the mockup test confirmed the reliability of the robot for the characterization of the mockup properties. Stiffness of the tested springs was accurately quantified with an error of less than 1.6 Nm/rad in any of the tested conditions. A pilot study with 5 human subjects further confirmed that the robot could be successfully used to quantify multi-dimensional human shoulder impedance in both pitch and yaw directions with high reliability ($R^2 > 0.97$). The average human shoulder stiffness and damping at around the neutral arm posture under low muscle activation (< 5% maximum voluntary contraction) were 30.9 Nm/rad and 3.0 Nms/rad, respectively.**

I. INTRODUCTION

The human shoulder plays a vital role in the functionality and performance of the arm. As the basis of upper limb motion, its health is of the utmost importance in the completion of daily tasks. Impairment of the shoulder, caused by stroke or other forms of neurological disease, can be extremely detrimental to a patient's quality of life. One of the primary reasons for this is that position errors in shoulder orientation accumulate and propagate to the elbow and wrist, affecting the performance of the entire arm [1]. This is why rehabilitation of the shoulder is a primary focus for many clinicians.

One of the primary causes of neurologically impaired shoulder performance is abnormal mechanical impedance, which is a fundamental property of the human neuromusculoskeletal system that enables natural and seamless physical interaction [2]. Joint mechanical impedance, or simply joint impedance, can be accurately modeled as a 2nd order system consisting of spring, damper and inertia [3]. In particular, quantifying the stiffness and damping of the shoulder for both healthy and impaired subjects could help to improve our collective understanding of how neurological disease affects upper limb performance [4]-[6]. This improved understanding could even lead to better rehabilitation protocols for conditions such as stroke through better identification and targeting of neurological conditions, for example, damping-dependent spasticity and stiffness-dependent hypertonicity [7].

Despite its importance, there is a fundamental knowledge gap in the understanding of shoulder impedance, mainly due to a lack of appropriate characterization tools. Perhaps the most prominent studies that examine shoulder impedance are performed using a single-axis servo that attaches to the human arm. The device can be manually re-positioned to characterize the impedance in either the pitch or yaw directions [8]. The device works by perturbing the human arm and measuring the corresponding position and interaction force/torque in order to estimate shoulder stiffness and damping properties. While this pioneering research has helped lay the groundwork for shoulder impedance studies, it has limitations inherent to the hardware setup. First, the device has limited workspace, which makes it difficult to test a variety of postures. Second, it does not allow for multi-dimensional perturbations without changing the entire device's setup. These multi-dimensional perturbations are necessary to develop a more complete picture of shoulder impedance. Finally, the limited active degree-of-freedom (DoF) of the device makes characterization during dynamic movement tasks difficult. This is because the single DoF must be aligned with direction of motion, which means off-axis perturbations are not possible during dynamic testing.

Utilizing a higher DoF robot architecture could be used to overcome many of these disadvantages listed above, however doing so would introduce new problems. The most prominent of these would be the added inertia. One of the reasons why the authors in the previously mentioned works opted for such a simplistic robot to perform these experiments is that the single-axis servo architecture has relatively low inertia. This is critical for providing high speed perturbations. High speed perturbations are necessary to characterize the intrinsic and reflex characteristics of joint impedance [9], [10]. Traditional serial robots have too much architecture-dependent inertia to provide fast perturbation for reliable impedance characterization [11]. Parallel robots have inherently low inertia and could likely meet the acceleration requirements

Research supported by National Science Foundation Award #1846885 and #1925110.

Dongjune Chang, Justin Hunt, John Atkins, and Hyunglae Lee are with School for Engineering of Matter, Transport and Energy, Arizona State University, Tempe, AZ 85287, USA {dongjune.chang, jphunt3, jatkin15, hyunglae.lee}@asu.edu; 480-727-7463. *: corresponding author

necessary to perform this research [11], [12]. However, parallel robots have a limited workspace, and many do not interface well with the human biology [13]. Overcoming these limitations are necessary and was the motivation behind prior works [14], [15]. In these works, the authors introduced a novel 4-bar spherical parallel manipulator (4B-SPM) that could interface well with complex biological joints like the shoulder, hip, wrist and ankle joints. The authors demonstrated this new parallel architecture by developing a shoulder exoskeleton prototype meant for characterizing multi-dimensional shoulder impedance [16].

In order to characterize human shoulder impedance using the 4B-SPM shoulder exoskeleton, its performance must first be evaluated. To do this, a set of experiments are performed using a physical shoulder mockup with adjustable mechanical properties. Additionally, some pilot human experiments were performed to show the robot's ability to be used by human subjects without issue while collecting all necessary data for impedance quantification. This pilot human experiments were performed at around a single neutral arm posture, defined as follows: shoulder in ~45° of abduction, ~45° of horizontal flexion, and the elbow in ~90° of flexion. Not only will this work help determine the validity of the new 4B-SPM architecture for the purposes of human joint impedance characterization, but it will provide a valuable tool for helping us to know how the neuromechanics of the human shoulder operate.

The rest of this paper describes the efforts made to validate the shoulder exoskeleton for human impedance studies, along with some preliminary results from human testing. The sections are organized as follows: Section II includes hardware setup, procedures for mockup tests and human tests, and data analysis methods. Section III details the results of the mockup tests and the pilot human tests. Finally, Section IV concludes the paper with a discussion and summary of the contribution.

II. Methods

A. Hardware Setup: Shoulder Exoskeleton

The 4B-SPM shoulder exoskeleton used in this work utilizes three actuated 4-bar substructures that operate about a central point designated as the center of rotation of the shoulder (Fig. 1). The three 4-bar substructures work synergistically to decouple and control the roll, pitch and yaw of a shoulder plate that rotates about the center point, i.e., the center-of-rotation of the shoulder.

Each 4-bar substructure contains two servos (Dynamixel MX-106R, Robotis, South Korea) that control the roll and pitch DoF. The roll axis of each substructure intersects at the central point. The top linkage in each 4-bar substructure is extended to reach the shoulder plate that moves tangential to a virtual sphere which encapsulates the shoulder joint. The radius of this virtual sphere is equal to the length of the vertical set of parallel linkages in each 4-bar. Each top linkage is connected to the shoulder plate using a spherical joint. Mounted to the shoulder plate is a 6-axis force/torque (F/T) transducer (AXIA 80 EDU, ATI-AI, NC, USA).

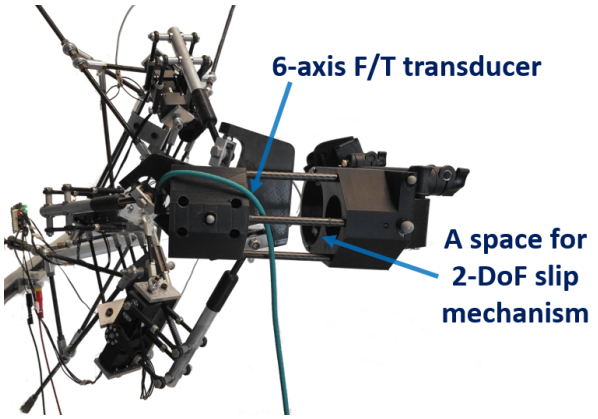

Fig. 1. Overall view of the 4B-SPM shoulder exoskeleton mounted to a stand. Notable features include: (1) 2-DoF 4-bar actuated substructure (one of three), (2) Shoulder plate with embedded 6-axis force/torque transducer, (3) Upper arm cuff with an embedded 2-DoF slip mechanism and a blood pressure cuff for an adjustable compliant human-robot interface.

Mounted to the opposite side of the transducer is a set of parallel carbon fiber rods that are in turn connected to the outer shell of an upper arm cuff that couples the exoskeleton to a human subject. The inner shell of the upper arm cuff consists of a blood pressure cuff housed within an aluminum piece of tubing. The blood pressure cuff is used in order to maintain a consistent fit across subjects with different arm diameters.

In order to account for a possible joint misalignment between the exoskeleton robot and human subject, the inner aluminum shell is permitted to slip relative to the outer shell. The slip is possible due to a series of roller bearings embedded within the internal surface of the outer shell. More information regarding the 4B-SPM shoulder exoskeleton can be found in the authors' prior works [14], [16].

The Euler angle position of the exoskeleton's cuff can be tracked using onboard encoder feedback. However, in prior works it was shown that encoder feedback for this prototype is only accurate to within 1°, due to tolerancing during fabrication [16]. Therefore, to achieve a higher accuracy in the position data needed to estimate shoulder impedance, a 3D motion capture system (Bonita 10 System, Vicon, UK) was added to track the position of the robot and/or human subjects.

B. Hardware Setup: Physical Shoulder Mockup

In order to ensure that the 4B-SPM shoulder exoskeleton robot is capable of correctly estimating the properties of the human shoulder, in particular shoulder impedance, a series of tests were first performed using a physical shoulder mockup.

The mockup was constructed using a 6 mm threaded steel rod attached to a steel tie-rod joint. The tie rod joint was attached at the center-of-rotation of the exoskeleton by way of a steel mounting fixture. This point is also the theoretical center-of-rotation for the shoulder of human subjects. The rod was secured within the upper arm cuff of the exoskeleton using a fitted wooden block.

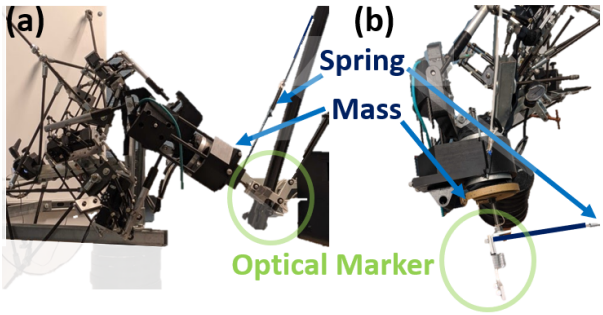

Fig. 2. The 4B-SPM shoulder exoskeleton setup interfacing with a physical shoulder mockup that has adjustable inertia and stiffness properties. In this example, the mockup is equipped with a 0.07 kgm^2 (i.e., 1 kg) mass and a 24.4 Nm/rad spring oriented in (a) the pitch direction (side view) and (b) yaw direction (top view).

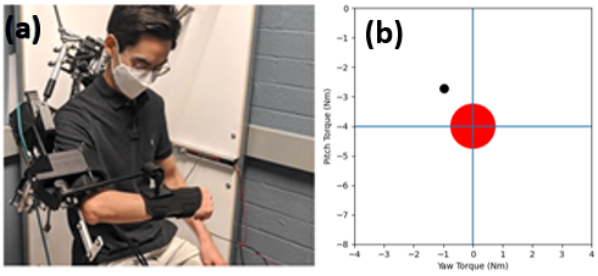

Fig. 3. (a) The 4B-SPM shoulder exoskeleton setup interfacing with a human subject. A locking fixture was added to secure the orientation of the forearm during experiments. The human experiment was performed where the subject's arm is in a neutral position. (b) User torque feedback display showing current and reference torques in pitch and yaw directions.

To test different inertia and stiffness properties, a set of calibrated masses and springs were used. The masses were attached by sliding them over the threaded rod and securing them with nuts and washers. The springs were attached at one end to the mockup using copper cabling. The other end of the springs was fixed to a point on the ceiling or wall using the same type of copper cabling. The orientation of the copper cabling was positioned such that the springs act orthogonal to the mockup at the initial test position. This setup is shown in Fig. 2.

Springs were chosen that reflect stiffness estimates in the range of what is expected for human subjects. These values were 20-50 Nm/rad in near relaxed state [8]. Two different mass conditions (0 kg and 1 kg) were chosen to evaluate the sensitivity of stiffness estimation to varying inertia conditions. Dampers were not used in these mockup experiments. The reason for this is that pure dampers are a theoretical concept. However, due to the close relationship between position, velocity and acceleration, accurate estimates of position-dependent stiffness and acceleration-dependent inertia would suggest that the related velocity-dependent damping would also be reasonably estimated in human experiments.

The spring and mass conditions for these tests are as follows: (1) 24.4 Nm/rad with 0 kg added, (2) 24.4 Nm/rad with 1 kg added, (3) 42.3 Nm/rad with 0 kg added, and (4) 42.3 Nm/rad with 1 kg added.

C. Experiments: Physical shoulder mockup

To estimate the known inertia and stiffness for different combinations of masses and springs, perturbations were applied to the mockup via the 4B-SPM shoulder exoskeleton. During these perturbations, the onboard force/torque sensor recorded interaction forces and torques, while the offboard motion capture system tracked the position of the mockup. The data cycle time was recorded and used in conjunction with position to determine velocity and acceleration of the mockup. With torque, position, velocity, and acceleration known, multi-input single-output linear regression was used to determine inertia (I), damping (B) and stiffness (K) of the mockup. In the case of these experiments, both I and K are known and can be used to verify that the system is accurately estimating inertia and stiffness.

The 4B-SPM shoulder exoskeleton was commanded to perturb in two directions: negative pitch and yaw. These directions were selected as they represent two independent (i.e. decoupled) Euler angles. A 5th order minimum jerk perturbation profile was used for each direction. Each perturbation had a commanded amplitude of 7° and rise time of 160 ms, and 50 perturbations were performed in each direction of negative pitch and negative yaw. To account for any variabilities from a procedure setting the shoulder mockup, 5 experiments were performed in separate days for each mass/spring condition. Since there were 2 directions tested, with 4 different mockup conditions and 5 repetitions of each condition, a total of 40 tests were performed with the mockup.

D. Experiments: Human Subjects

In order to evaluate the practical ability of the 4B-SPM shoulder exoskeleton to collect the necessary data needed to estimate the human shoulder impedance, a series of experiments were performed with human subjects. In these experiments, the human subjects were seated on an adjustable chair with their arm connected to the robot.

Before the experiment started, 3 wireless surface electromyography (EMG) electrodes (Delsys Trigno, MA, USA) were attached to the subject's right shoulder and EMG data was collected for the three muscles of interest: anterior deltoid (AD), medial deltoid (MD), and posterior deltoid (PD). For each muscle group, maximum voluntary contraction (MVC) was calculated by taking the maximum signal from the maximum exertions recorded. The MVC data was used as a reference to quantify the level of muscle activation during the experiment.

In order to track arm orientation, a rigid L-shaped frame with 3 optical markers was attached to the subject's right arm between the wrapped blood pressure cuff. The cuff allows adjustment for the human-robot interface so that subjects with arms whose diameter is smaller than the diameter of the robot's arm cuff (shown in Fig. 1) can be well secured to the robot. Then the subject was asked to wear the cylindrical metal tube and place their arm in the robot's slip mechanism.

The height of the chair and position of the human shoulder were adjusted such that they are comfortable, and the center-of-rotation of the robot and the theoretical center-of-rotation

TABLE I. PHYSICAL SHOULDER MOCKUP RESULTS

Negative Pitch Direction						Negative Yaw Direction					
Condition	Coefficient	Expected	Mean	Std	R^2	Condition	Coefficient	Expected	Mean	Std	R^2
0kg, Spring 1	Stiffness	24.40	22.79	1.98	0.998	0kg, Spring 1	Stiffness	24.40	24.84	1.94	0.990
	Damping	-	-0.004	0.009			Damping	-	0.150	0.148	
	Inertia	0.070	0.063	0.001			Inertia	0.070	0.077	0.004	
0kg, Spring 2	Stiffness	42.30	43.44	2.48	0.996	0kg, Spring 2	Stiffness	42.30	43.44	2.48	0.996
	Damping	-	0.037	0.098			Damping	-	0.037	0.098	
	Inertia	0.070	0.076	0.004			Inertia	0.070	0.076	0.004	
1kg, Spring 1	Stiffness	24.40	23.29	3.31	0.985	1kg, Spring 1	Stiffness	24.40	23.29	3.31	0.985
	Damping	-	0.468	0.276			Damping	-	0.468	0.276	
	Inertia	0.137	0.149	0.007			Inertia	0.137	0.149	0.007	
1kg, Spring 2	Stiffness	42.30	43.07	3.25	0.997	1kg, Spring 2	Stiffness	42.30	43.07	3.25	0.997
	Damping	-	0.141	0.212			Damping	-	0.141	0.212	
	Inertia	0.137	0.160	0.004			Inertia	0.137	0.160	0.004	

* Stiffness: Nm/rad, Damping: Nms/rad, Inertia: kgm^2

of the human shoulder are as accurately co-located as possible. The locking fixture was then adopted to maintain the orientation of the forearm during the experiment. The experiment was conducted such that the human arm is in a neutral position (shoulder in ~45° of abduction, ~45° of horizontal flexion, and the elbow in ~90° of flexion) seen in Fig. 3 (a) to best measure the shoulder impedance in a natural and comfortable state.

The total experiment consisted of 8 blocks, with 12 perturbations in each block. Separating these 8 blocks prevented the human arm from getting fatigued and thus altering results. After each block, a minimum of 2-minute break was given to the subject. Each block consisted of 3 perturbations in each of the 4 directions applied in random order for a total of 12 perturbations.

In order to prevent the human arm from applying excessive force to the robot during a perturbation and prevent the subject from leaning on the robot, conditions for triggering perturbation were introduced. The subject was asked to watch a visual feedback display shown in Fig. 3(b) and place a black dot (current interaction torque values in pitch and yaw directions) in a larger circle (reference torque measured in a pre-session when the subject maintained the neutral arm posture without any robot support against gravity). The larger circle turned red if the torque components in the pitch and yaw directions are far from the reference torque values. If the current torque components remain in the boundary of the reference torque values for a random amount of time (1–2 s), a perturbation was triggered in one of the 4 perturbation directions: positive pitch, negative pitch, positive yaw, and negative yaw. A fast ramp-and-hold perturbation with an amplitude of 5° and rise time of 160 ms was used.

Five young, healthy subjects (age: 21–41, height: 172–192 cm, weight: 60–88.5 kg, sex: 5 males) participated in this study, which was approved by the Institutional Review Board of Arizona State University (STUDY00009059). Subjects provided informed, written consent prior to participation. All experimental procedures were performed in accordance with the relevant guidelines and regulations.

E. Post-Processing

The raw data collected from the mockup and human experiments included motion capture marker data for the exoskeleton itself and the markers attached to the mockup or the human subject as well as 6-axis force and torque data sampled at 250 Hz. Both the torque and marker data were low pass filtered using a bi-directional 4th order Butterworth filter with a cutoff frequency of 12 Hz.

The Euler angles were extracted from the marker data by constructing a rotation matrix from the normalized differences in the markers and taking cross products with the global z-axis set in the 3D motion capture system. This allows the roll axis of the human marker data to be decoupled from the pitch and yaw directions, allowing for better estimation of the pitch and yaw angles alone. Then for each trial, the Euler angles were baselined such that the Euler angles began the trials at a 0° offset. Since the perturbations apply a purely planar rotation, the angular velocity and acceleration were found by taking first order discrete-time derivatives of the Euler angles.

Outlier rejection on the trials was performed to remove highly variable trials from excessive human movement during the perturbation. The criteria for what was classified as an outlier was such that any single trial where the acceleration profile left a running mean +/- 2.5 standard deviation (std) range calculated from all collected trials.

Stiffness, damping and inertia coefficients were calculated by fitting a simple linear regression from all non-failed trials using the linear statistical model (Eq. (1)):

$$\tau_i = \beta_0 + \beta_1\theta_i + \beta_2\dot{\theta}_i + \beta_3\ddot{\theta}_i + \epsilon_i \quad (1)$$

where τ_i is the measured torque, β_0 is the intercept coefficient, β_1 is the stiffness coefficient, β_2 is the damping coefficient, β_3 is the inertial coefficient, and ε_i is the unknown error term all at the i^{th} observation. The human experiment data was processed similar to the mockup data but uses constrained linear regression. Constraints on the regression coefficients

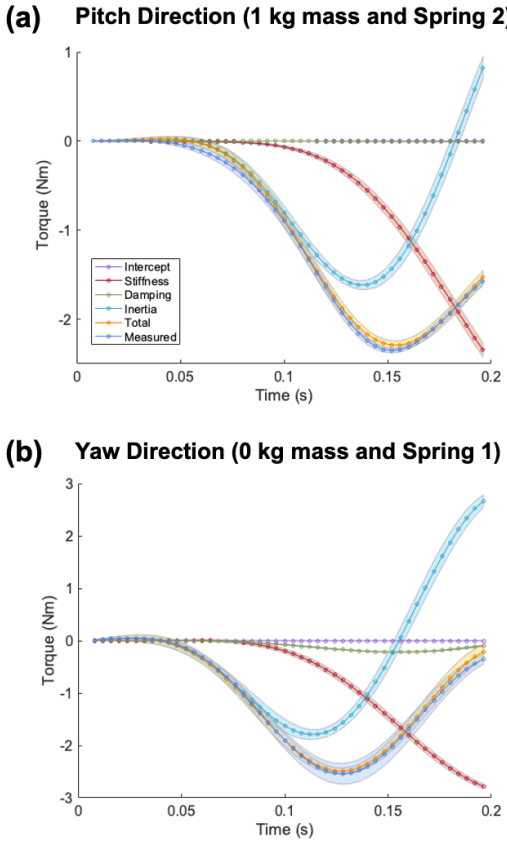

Fig. 4. Sample results of the physical shoulder mockup experiments. Measured torque with the estimated torque contributions from the kinematic data and regression coefficients (stiffness, damping, and inertia) for (a) the negative pitch and (b) negative yaw directions. The mean and mean±1 std from the 5 repeated experiments are presented in solid lines and color bands, respectively.

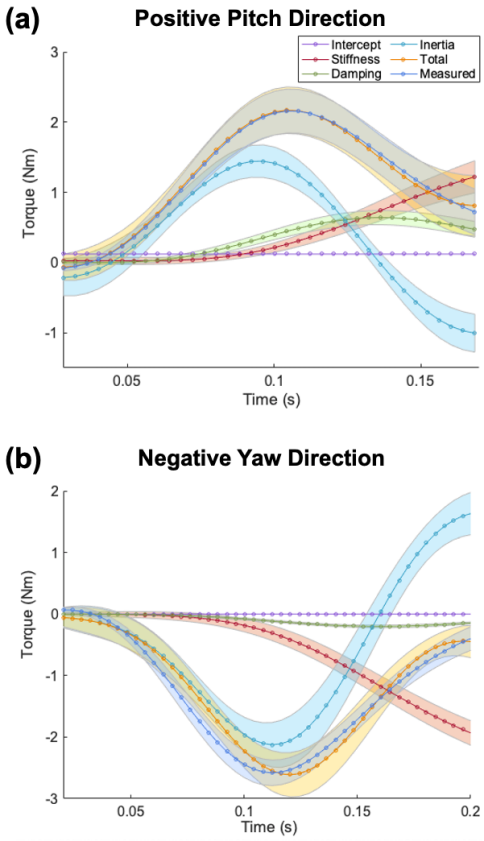

Fig. 5. Results of a representative subject in the human experiments. Measured torque with the estimated torque contributions from the kinematic data and regression coefficients (stiffness, damping, and inertia) for (a) the positive pitch and (b) negative yaw directions. The mean and mean±1 std from the 24 repeated measurements are presented in solid lines and color bands, respectively.

were applied such that stiffness and damping must be non-negative. The chosen fitting window for the human trials was set between the maximum calculated acceleration and the minimum acceleration. This window was chosen in order to minimize any compliance effects from the coupling of the robot and human.

EMG data was processed by first subtracting the mean of the signals to remove the constant offset (DC offset), then rectifying the signals, and then lowpass filtering with a bi-directional 4th order Butterworth filter with a cutoff frequency of 5 Hz. The percentage MVC (%MVC) was then calculated for each trial by normalizing the EMG signals by the MVC. In order to quantify muscle activation at the time of impedance quantification, the EMG amplitude was calculated in a time window of 200 ms prior to each perturbation (-200−0 ms).

III. Results

A. Physical shoulder mockup experiments

The mockup experiments showed the very high reliability of the robot for the quantification of mockup impedance parameters, i.e., stiffness, damping and inertia. The R^2 value for all linear regression fits were higher than 0.985 (Table I). Measured torque (orange) matched well with the estimated torque by summing the torque contributions of three impedance parameters (blue) (Fig. 4). The torque response of the system shows a consistent pattern of inertial effects dominating the system at the start of the perturbation while the stiffness contributions grow until the end of the fitting window. This trend is to be expected based on the shape of the kinematic response. The sum of these torque contributions carefully follows the measured torque throughout the perturbation, showing that the fitted parameters do not show a strong time dependency over the fitting window which is expected for this passive system. In addition, the mockup experiments were clearly highly repeatable as seen from the low variance over 5 repeated experiments.

Group average results of 5 repeated experiments confirmed that expected stiffness of the two tested springs under two different inertia conditions was accurately estimated by the fitted linear regression model (Table I). The error was less than 1.6 Nm/rad in any of the tested conditions. The damping terms were all small compared to the other terms and the inertia was close to the expected values. In general,

TABLE II. GROUP AVERAGE RESULTS OF THE HUMAN SHOULDER IMPEDANCE QUANTIFICATION EXPERIMENTS

Perturbation direction	Coefficient	Mean	Std	R^2
Positive Yaw	Stiffness	20.33	11.03	0.972
	Damping	2.61	1.69	
	Inertia	0.17	0.03	
Negative Yaw	Stiffness	24.73	19.48	0.978
	Damping	3.96	1.90	
	Inertia	0.17	0.02	
Positive Pitch	Stiffness	24.34	11.53	0.982
	Damping	2.95	1.43	
	Inertia	0.12	0.03	
Negative Pitch	Stiffness	54.13	16.51	0.985
	Damping	2.53	0.82	
	Inertia	0.11	0.02	

* Stiffness: Nm/rad, Damping: Nms/rad, Inertia: kgm^2

these results are very close to the expected values for both directions, giving high confidence in the accuracy of the values.

B. Human subject experiments

The human experiments demonstrated that the robot could be successfully utilized to quantify human shoulder impedance with high reliability in both pitch and yaw directions. Results of a representative subject showed that the measured (orange) and estimated (blue) torque contributions in both the positive pitch and negative yaw directions match well (Fig. 5).

The torque contributions from the fitted kinematic data show the same pattern observed in the mockup experiments, with strong inertial contributions at the beginning of the perturbation and the stiffness growing later in time. The major difference is the presence of damping and higher variance due to the coupling of a human subject, but the sum of the torque contributions by stiffness, damping and inertia terms always remains close to the measured torque over the fitting window. This suggests time dependency of the impedance characteristics is small over the duration of the perturbation.

Group average results of 5 subjects further confirmed the reliability of impedance quantification (Table II). The R^2 value for all linear regression fits are higher than 0.972 in all 4 tested directions. There is also a strong agreement in the inertia estimates for both yaw direction cases and both pitch direction cases, which supports the reliability of quantification. In the tested arm posture, i.e., the neutral arm posture, higher arm inertia about the shoulder joint is to be expected in the yaw direction than the pitch direction and the experimental results confirmed this.

The estimated stiffness was mostly homogenous (20−25 Nm/rad) in all perturbation directions except the negative pitch perturbation direction (54.1 Nm/rad). This result is to be expected since the robot did not provide weight support against gravity and the measurement was performed when the subjects maintained the neutral arm posture by slightly exerting shoulder torque in the positive pitch direction, which is opposite to the direction of negative pitch perturbation.

The level of muscle activation during the experiments was relatively low. When averaged across the 5 subjects, the mean (and std in parentheses) EMG amplitude before perturbation (-200−0 ms) was 4.3 (3.3), 3.0 (1.9), 2.3 (0.9) %MVC for AD, MD, and PD, respectively. Given the selected neutral arm posture with shoulder abduction of ~45° and horizontal flexion of ~45° and without gravity compensation from the robot, higher muscle activation of AD and MD than PD is expected.

The variance of the stiffness estimates was higher than the similar tests for the mockup experiments, but this is largely due to inter-subject variation in natural stiffness as well the degree of compliance in the human-robot interface from differences in arm shape.

The estimated damping was largely stationary for all directions with the negative yaw direction being a slight exception. The expected damping is difficult to quantify, but these close estimates for all 4 directions coupled with the high R^2 suggest an accurate characterization of damping for these 5 subjects.

IV. DISCUSSION

This work aimed to determine the validity of using the novel 4B-SPM shoulder exoskeleton robot for the purpose of characterizing the multi-dimensional (specifically in pitch and yaw directions) mechanical impedance of the shoulder joint, and exemplified the robot by the accuracy in the estimates of mechanical impedance of both a physical shoulder mockup with known mechanical properties and the actual shoulder of human subjects.

The results of the mockup experiments ($R^2 > 0.985$) led to the conclusion that the robot is in fact capable of estimating stiffness and inertia accurately. As previously mentioned, damping could not be tested due to the fact that pure dampers do not exist. Instead, it is postulated that due to the relationship between position, velocity and acceleration, it is reasonable to assume that accurate estimates of position-dependent stiffness and acceleration-dependent inertia, would suggest the velocity-dependent damping should be reasonably estimated. This is supported by the fact that the mockup tests yield a near zero damping estimate, which is expected from the very low friction design of the mockup, and the human damping estimates agree for all tested directions.

The results of the human experiments ($R^2 > 0.972$) further extend the confidence and reliability of impedance estimates from the mockup testing to human trials based on comparisons of the resultant stiffness and damping to that of prior works [8]. Across the 5 subjects tested in this study, each of the shoulder impedance parameters fell within the expected values.

This work suggests that the 4B-SPM architecture is in fact a viable option for the development of exoskeleton devices for the purposes of interfacing with complex biological joints, including the shoulder. This work also demonstrates that the 4B-SPM shoulder exoskeleton robot is a promising new tool for the purpose of characterizing multi-dimensional human shoulder impedance. While these early tests of human shoulder impedance are not fully conclusive, they do provide a starting point in experimental protocol that will lead to more extensive future work including quantification in various arm postures and during dynamic movement tasks.

REFERENCES

[1] R. M. Enoka, *Neuromechanics of human movement*. Human kinetics, 2008.

[2] J. J. Palazzolo, M. Ferraro, H. I. Krebs, D. Lynch, B. T. Volpe, and N. Hogan, "Stochastic estimation of arm mechanical impedance during robotic stroke rehabilitation," *IEEE Trans. Neural Syst. Rehabil. Eng.*, vol. 15, no. 1, pp. 94–103, 2007.

[3] N. Hogan, "Mechanical impedance of single-and multi-articular systems," in *Multiple muscle systems*, Springer, 1990, pp. 149–164.

[4] D. T. Wade, R. Langton-Hewer, V. A. Wood, C. E. Skilbeck, and H. M. Ismail, "The hemiplegic arm after stroke: measurement and recovery.," *J. Neurol. Neurosurg. Psychiatry*, vol. 46, no. 6, pp. 521–524, 1983.

[5] V. M. Parker, D. T. Wade, and R. L. Hewer, "Loss of arm function after stroke: measurement, frequency, and recovery," *Int. Rehabil. Med.*, vol. 8, no. 2, pp. 69–73, 1986.

[6] A. Heller, D. T. Wade, V. A. Wood, A. Sunderland, R. L. Hewer, and E. Ward, "Arm function after stroke: measurement and recovery over the first three months.," *J. Neurol. Neurosurg. Psychiatry*, vol. 50, no. 6, pp. 714–719, 1987.

[7] C. Marciniak, "Poststroke hypertonicity: upper limb assessment and treatment," *Top. Stroke Rehabil.*, vol. 18, no. 3, pp. 179–194, 2011.

[8] D. B. Lipps, E. M. Baillargeon, D. Ludvig, and E. J. Perreault, "Quantifying the Multidimensional Impedance of the Shoulder During Volitional Contractions," *Ann. Biomed. Eng.*, pp. 1–16, 2020.

[9] E. J. Perreault, P. E. Crago, and R. F. Kirsch, "Estimation of intrinsic and reflex contributions to muscle dynamics: a modeling study," *IEEE Trans. Biomed. Eng.*, vol. 47, no. 11, pp. 1413–1421, 2000.

[10] J. Shemmell, M. A. Krutky, and E. J. Perreault, "Stretch sensitive reflexes as an adaptive mechanism for maintaining limb stability," *Clin. Neurophysiol.*, vol. 121, no. 10, pp. 1680–1689, 2010.

[11] O. Khatib, "Augmented object and reduced effective inertia in robot systems," in *1988 American Control Conference*, 1988, pp. 2140–2147.

[12] S. Briot, W. Khalil, and others, "Dynamics of parallel robots," *From rigid bodies to Flex. Elem. Springer*, 2015.

[13] J.-P. Merlet, "Jacobian, manipulability, condition number, and accuracy of parallel robots," 2006.

[14] J. Hunt and H. Lee, "A New Parallel Actuated Architecture for Exoskeleton Applications Involving Multiple Degree-of-Freedom Biological Joints," *ASME J. Mech. Robot.*, vol. 10, no. 5, p. 051017, Aug. 2018, doi: 10.1115/1.4040701.

[15] J. Hunt and H. Lee, "Four-bar parallel actuated architecture for exoskeleton." US Patent Application 16/387,152. 2019

[16] J. Hunt and H. Lee, "Development of a Low Inertia Parallel Actuated Shoulder Exoskeleton Robot for the Characterization of Neuromuscular Property during Static Posture and Dynamic Movement," in *2019 International Conference on Robotics and Automation (ICRA)*, 2019, pp. 556–562.